Proc. 5th International Conf. on High Energy Rate Fabrication, Denver Research Institute, Denver, June, p.1.4.1 (1975).

A "WAVY WAVE" MODEL FOR THE SHOCKING OF POLYCRYSTALLINE METALS

MARC A. MEYERS

Centro de Pesquisa de Materiais, Instituto Militar de Engenharia, Pça. Gen. Tibúrcio, Urca, ZC-82, Rio de Janeiro,RJ,Brasil.

Abstract

It is shown, by means of mathematical calculations conducted for a simplified model, that the shock wave takes a special configuration in polycrystalline metals. It is characterized by irregularities in the front position, peak pressure and continuous emission of reflected waves. Consequently, a "wavy wave" configuration results. These irregularities generate, at a mean pressure of 300 Kbar, shear stresses on planes perpendicular to the shock front that exceed the dynamic yield stress of metals. It is therefore suggested that the "wavy wave" has an effect on the residual substructure of the metal.

1. INTRODUCTION

The residual substructures due to the passage of shock waves through metals have been widely studied. Some interactions between the shock wave and existing defects have been considered (1-4). However, in all cases the assumption of a planar wave is implied.

Among the factors influencing the residual substructure of shock hardened metals, the peak pressure, pulse duration (5-8), rarefaction rate (9) and rate of decay of the pulse width (9) are usually recognized as being the most important.

It is the purpose of this paper to show that the interactions between the shock wave and a polycrystalline metal affect the shape of the shock wave and, consequently, the parameters governing the residual substructure. In addition, the interactions between the wave and existing defects should be affected by the modified shock wave.

Three interactions are considered:

a) Different crystallographic orientations exhibit different shock-wave velocities.

b) Peak pressures are dependent upon crystallographic orientation,

c) Reflected waves are produced when the shock wave traverses different grains; this is the result of impedance dependance upon crystallographic orientation.

These interactions will be analysed, with the necessary simplifying assumptions being introduced and justified. No differential temperature effects will be considered. A simplified realistic model will be considered: a nickel sheet with average grain size of 10 μm subjected to a shock wave with a mean pressure of 300 Kbar and pulse duration of 1 μsec.

2. CALCULATIONS

2.1 Irregularity of the Shock Front

The propagation velocity of shock waves can be obtained from the velocity of dilatational elastic waves, with the assumption of zero shear modulus. This simplification is usually introduced in order to allow the use of the hydrodynamic theory. This yields(10):

$$U = \left(\frac{K}{\rho} \right)^{1/2} \qquad (1)$$

where K is the bulk modulus and ρ the material density at the peak pressure. Elastic-plastic treatments have been developed(11) but would render the treatment too complex. Equation (1) is derived from expressions where the assumption of isotropy is made.

In anisotropic materials the velocity of plastic wave is dependent upon crystallographic orientation. Johnson(12) calculates them by taking into account shear strength effects and, consequently, the various slip planes and directions involved. However, for the purpose of the calculations presented herein it suffices to take the elastic wave velocities and assume zero shear strength. The longitudinal components of the velocities of elastic waves for cubic materials along the three crystallographic orientations <100>, <110> and <111> are presented by Ghatak and Kothari (13) in terms of the elastic stiffnesses c_{11}, c_{12}, c_{44} and the material density:

$$U_{<100>} = \sqrt{\frac{c_{11}}{\rho}} \qquad (2)$$

$$U_{<110>} = \sqrt{\frac{c_{11} + c_{12} + 2c_{44}}{\rho}} \qquad (3)$$

$$U_{<111>} = \sqrt{\frac{c_{11} + 2c_{12} + 2c_{44}}{3\rho}} \qquad (4)$$

The velocities of the longitudinal plastic waves are obtained from the assumption that the material cannot resist shear stresses, i.e., that $c_{44} = 0$. For nickel the values of the stiffnesses are (13), at 300°K:

$$c_{11} = 2.508 \times 10^{12} \text{ dynes/cm}^2$$

$$c_{12} = 1.500 \times 10^{12} \text{ dynes/cm}^2$$

The density of nickel at 300 Kbar is given by its Hugoniot curve and is equal to 10 g/cm^3. It is assumed that there is no transient temperature rise associated with the passage of the shock wave. Hence, the velocities are:

$$U^P_{<100>} = U_1 = 5.01 \times 10^5 \text{ cm/sec}$$

$$U^P_{<110>} = U_2 = 6.39 \times 10^5 \text{ cm/sec}$$

$$U^P_{<111>} = U_3 = 4.29 \times 10^5 \text{ cm/sec}$$

It can be seen that the velocity of the shock wave in the <110> direction is 50% higher than in the <111> direction.

The shock-wave profile can be estimated at any position inside the nickel sheet, in various degrees of rigorousness. An approximate profile that does not require extensive mathematical manipulation can be produced by making some simplifying assumptions and specifying some parameters:

a) All grains are cubes with 0.001 cm sides, arranged in horizontal layers, as shown in Figure 1. There is no exact superposition of the cubes. The shock wave is horizontal and traverses the material from top to bottom.

b) It is assumed that there are only three vertical orientations for the grains: <100>, <110> and <111>. They are coded 1,2, and 3, respectively. These are the sole orientations along which purely longitudinal waves exist (13,14). Assuming that the least texturing takes place, they will be present in proportion to their multiplicity factors; these are 6, 12 and 8, respectively. Consequently, the probabilities for the orientation of each grain are:

$$P_{<100>} = p_1 = 0.461$$

$$P_{<110>} = p_2 = 0.231$$

$$P_{<111>} = p_3 = 0.308$$

c) The shock-wave velocity, particle velocity, peak pressure and density are mutually interdependent and related through the Rankine-Hugoniot relations. However, it will be assumed in

this section that the nickel density and plastic wave velocities are constant, regardless of small variations in the peak pressure. This assumption is justified in Section 2.2.

d) The wave profile will be estimated at 0.01 cm below the surface, or when the mean of the wave has traversed 10 grains.

Based on these assumptions, the problem can be solved in two stages. Firstly, what will be sought is the probability distribution function of the transit times for 0.01 cm. Secondly, this direction will be converted into a position distribution function and then into a profile. The problem can be statistically stated as: what is the probability distribution function of 10 indistinguishable events 1,2 and 3, with probabilities p_1, p_2 and p_3, and values t_1, t_2 and t_3? The values t_1, t_2 and t_3 are the transit times for the three grain orientations:

$$t_{<100>} = t_1 = \frac{0.001\text{cm}}{U_1} = 2.00\text{x}10^{-9} \text{ sec} \quad (5)$$

$$t_{<110>} = t_2 = \frac{0.001\text{cm}}{U_2} = 1.57\text{x}10^{-9} \text{ sec} \quad (6)$$

$$t_{<111>} = t_3 = \frac{0.001\text{cm}}{U_3} = 2.31\text{x}10^{-9} \text{ sec} \quad (7)$$

Table 1 shows the 70 possible outcomes for the 10 events. In order to calculate the probabilities of the different outcomes, one has to determine the number of possible configurations for n_1 events of type 1, n_2 events of type 2, and n_3 events of type 3 ($n_1+n_2+n_3=10$). They are given by:

$$\frac{10\ !}{n_1\ !\ n_2\ !\ n_3\ !}$$

The probability for each of the configurations is given by:

$$p = (p_1)^{n_1} \times (p_2)^{n_2} \times (p_3)^{n_3} \quad (8)$$

The total transit time for each configuration is:

$$t = n_1t_1 + n_2t_2 + n_3t_3 \quad (9)$$

And the total probability is the product of the probability p by the number of possibilities in each configuration. As expected,

the sum of total probabilities is 1.

The possible outcomes, their transit times and probabilities are listed in Table 1. The traversal times are grouped in intervals of 0.3×10^{-9} sec and the probability distribution function is plotted in Figure 2. An approximate position distribution function, at the moment when the mean of the wave has traversed 10 grains, can be computed assuming a weighted average of velocities:

$$U_{av} = p_1 U_1 + p_2 U_2 + p_3 U_3 \qquad (10)$$

$$= 5.105 \times 10^{-5} \text{ cm/sec}$$

Multiplying this velocity by the limits of the time intervals, one obtains the positions. The upper abcissa in Figure 2 provides the distribution of these positions. It is to be noted that the above calculation is merely an approximation. However, sensible deviations only occur at the tails of the distribution of Figure 2; they are therefore of no great concern.

Figure 2 shows very clearly that the shock front is not a planar one. Deviations of the order of magnitude of 10 μm have a high probability. And, as the number of grains traversed increases, the distribution function will tend to broaden out into a progressively wider skewed Gaussian curve. However, there may be other effects, such as the generation of defects, impeding the progressive broadening; a steady-state distribution might therefore result.

2.2 Irregularity of the Peak Pressure

The analysis conducted in this section will use the same assumptions as Section 2.1.

When the copper driver plate impinges on the nickel sheet, it will produce a pressure pulse in the nickel sheet. In order for the mean pressure at the surface of the nickel sheet to be 300 Kbar, the velocity of the copper driver plate at the moment of impact has to be approximately $1{,}350 \times 10^2$ cm/sec. This value is obtained from the Pressure-Particle Velocity curves for nickel and copper. However, the Hugoniot curves for metals are experimentally determined and represent the values of polycrystalline aggregates. One would obtain different curves for different crystallographic orientations. To the author's knowledge, no such data are available for nickel. This orientation dependence of the response is directly responsible for the fluctuation in the peak pressure along the shock front. Since the curves are not available, they are estimated through some assumptions. The initial portion of a $P\text{-}V/V_o$ curve can be

approximated to a stress-strain curve, in spite of the different states of stress (uniaxial strain vs. uniaxial stress). So, the initial slope on the $P\text{-}V/V_o$ curve can be related to the elastic modulus of the material. This is shown in Figure 3. The full lines represent the Hugoniot curve and the elasticity modulus of a nickel polycrystalline aggregate. The straight line has a slightly higher slope than the initial portion of the Hugoniot curve, as expected (15). And, as the Young moduli for the different crystallografic orientations can be estimated from the elastic compliances (or stiffnesses) they can be used to estimate the Hugoniot curves for the different orientations. It is assumed that the slope of the $P\text{-}V/V_o$ curve is a characteristic of the material; it will however rotate around the ($P=0$, $V/V_o = 1$) point by angles equal to the angles between the Young moduli of the polycrystalline aggregate and the orientations <100>, <110> and <111>. The Young moduli are calculated from the elastic compliances (16) by a simple formula (17) and have been found to be:

$$E_{<100>} = E_1 = 1.36 \times 10^{12} \frac{\text{dynes}}{\text{cm}^2} = 1.36 \times 10^3 \text{ Kbar}$$

$$E_{<110>} = E_2 = 2.32 \times 10^{12} \frac{\text{dynes}}{\text{cm}^2} = 2.32 \times 10^3 \text{ Kbar}$$

$$E_{<111>} = E_3 = 3.04 \times 10^{12} \frac{\text{dynes}}{\text{cm}^2} = 3.04 \times 10^3 \text{ Kbar}$$

The Young modulus for annealed polycrystalline nickel is:

$$E = 2.07 \times 10^{12} \frac{\text{dynes}}{\text{cm}^2} = 2.07 \times 10^3 \text{ Kbar}$$

The three Hugoniot curves obtained by this method are shown in Figure 3. They can be transformed into Pressure-Particle Velocity curves by means of the Rankine - Hugoniot relations. The equation

$$u = \sqrt{-(P - P_o)(V - V_o)} \qquad (10)$$

where V and V_o are the final and initial specific volumes, and P and P_o the corresponding pressures provides the particle velocities for the various pressures. The resultant curves are shown in Figure 4. (The assumption of constant wave velocity for each orientation made in Section 2.1 can be justified by this plot. U is the slope of the segment joining the origin to a

certain pressure in the P-u curve. Changes in pressure, along a curve, will produce relatively small changes in U). For the sake of simplicity the copper driver plate is assumed to have a single characteristic P-u curve, equal to that of the polycrystalline aggregate. So, a copper particle velocity of $1{,}350 \times 10^2$ cm/sec, producing a mean pressure of 300 Kbar on the nickel polycrystalline curve, generates quite different pressures in the different grains. For the <100> orientation the pressure is 275 Kbar, for the <110> it is 308 Kbar and for <111> it is 332 Kbar. And, if one considers the Cu driver plate as made up of different grains with different Hugoniot curves, the differences would be even higher. The pressures would have the approximate range from 240 to 360 Kbar. As the wave traverses the first grain layer (see Figure 1) and enters the second layer, the various types of interactions have to be taken into account. This is shown in Table 2, where the pressures for the different orientations have been determined down to the third layer. One has to consider the P-u reflection curves for the three orientations and their intersections with the transmission curves. As the wave progresses through the successive grain layers, the same interactions have to be considered. This problem does not lend itself to an easy statistical analysis, as was the case for the shock-wave positions (Section 2.1). It suffices therefore to say that the distribution of pressures will be a composite of three distributions, with three means: 275, 308 and 332 Kbar. As the wave penetrates into the material, the distributions will tend to broaden.

2.3 Reflected Waves

Different crystallografic orientations have different shock impedances (ρ_o U), and reflected waves are consequently generated at all the boundaries between grains of different impedances. The peak pressure of the reflected wave is equal to the difference between the pressures in the two grains. They can be obtained from Table 2. So, reflections of 35, 60, 38, 27, 67, 32 Kbar are sent back to the first grain layer, from the boundary between the first and second layer. A rigorous analysis of the reflected waves would show that they contribute to change the peak pressures of the transmitted wave. However, this effect is not considered. The emission of reflected waves will continue at all the boundaries perpendicular to the shock direction. And, as the 10th grain layer is being traversed by the shock wave, the upper free surface of the nickel foil has been traversed by five reflected waves. Their magnitude is not negligible and they surely contribute to the overall residual strengthening of the metal.

3. CONCLUSIONS

Polycrystalline metals introduce several changes in the

characteristics of the shock wave. Three of these interactions are analysed for a realistic situation, a nickel sheet being impacted with a copper driver plate producing a pulse duration of 1 μsec and mean peak pressure of 300 Kbar. Their order of magnitude can be estimated. The main effects on the morphology of the shock wave are:

a) The shock front is irregular. After the mean of the wave has traversed 10 grains (100 μm) the positions of the front have a substantial spread (100 ± 10 μm).

b) The peak pressures are also irregular. The driver plate produces pressures of 275, 308 and 332 Kbar for the <100>, <110> and <111> orientations, respectively. As the wave propagates through the metal, a progressively broader distribution of pressure around these values develops itself.

c) The different shock impedances of the different orientations are responsible for the continuous production of reflection waves. These have peak pressures of up to 67 Kbar and can be reflected themselves.

Based on these anomalies a schematic model for the shock wave can be proposed. It is shown in Figure 5, at around 100 μm below the surface. Since the pulse duration is of 1 μsec, no rarefaction effects are noted. Along the penetration axis five irregularities can be seen. They correspond to the reflected waves. Secondary and higher order reflections have not been introduced. It is assumed, in Figure 1, that the different layers of grains are arranged in such a manner that there is no exact superposition of the cubes. This produces, in the model of Figure 5, a progressive refinement of the irregularities. As the wave traverses the first layers, they should be 10 μm wide. After 10 grains are traversed, the sucessive splitting will have reduced it to a mean of 1.0 μm. The model of Figure 5 is only an approximation to a real situation. In an actual polycrystalline metal, where a continuous distribution of orientations exists and the grain boundaries are not mutually perpendicular, the shock wave would have a slightly different appearance. The variation in both the shock front position and peak pressure would be continuous, and a "wavy wave" would result.

The irregularities of the shock wave introduce shear stresses along planes perpendicular to the shock front. These shear stresses are much higher than the dynamic yield strength of nickel. Their duration is such that they may introduce strain rates that are much lower than those encountered at planar shock fronts. Thus, although on a macroscopic scale polycrystalline metals can be considered as isotropic and shock waves regarded as planar, this assumption cannot be made on a microscopic scale, as shown by the wavy model presented herein. And since it is on a microscopic scale that the deformation mechanisms operate, this

effect should be of concern to metallurgists.

The treatment presented herein can be extended, with minor modifications, to the elastic precursor wave.

4. ACKNOWLEDGMENTS

This work was supported by the Brazilian Ministry of the Army and Office of Planning through IME Materials Research Center.

5. REFERENCES

1. C.H. Ma, Acta Met. 22, 675 (1974).

2. L.E. Murr, H.R. Vydyanath and J.V. Foltz, Met. Trans. 1, 3215 (1970).

3. P.A. Urtiew and R. Grover, J. Appl. Phys. 45, 140 (1974).

4. J.W. Taylor, J. Appl. Phys. 36, 3146 (1965).

5. A.S. Appleton and J.S. Wadington, Acta Met. 12, 956 (1964).

6. A.R. Champion and R.W. Rohde, J. Appl. Phys. 41, 2213 (1970).

7. A.P. Mantaroshin, G.M. Nagornov and P.O. Pashkov, The Phys. Met. and Metallogr. 29, 145 (1970).

8. L.E. Murr and M.L. Sattler, Scripta Met. 8, 1477 (1975).

9. R.N. Orava, South Dakota School of Mines and Technology, private communication (1974).

10. H. Kolsky, Stress Waves in Solids, p. 12, Dover Publications (1963).

11. E.H. Lee, Shock Waves and the Mechanical Properties of Solids, ed. J.J. Burke and V. Weiss, p. 3, Syracuse University Press (1971).

12. J.N. Johnson, J. Phys. Chem. Solids 35, 609 (1974).

13. A.K. Ghatak and L.S. Kothari, An Introduction to Lattice Dynamics, p. 67, Addison-Wesley Publishing Co. (1972).

14. W. Herrmann, D.L. Hicks and E.G. Young, Source cited in Ref. 11. p. 23.

15. O.E. Jones, Metallurgical Effects at High Strain Rates, ed. R.W. Rohde, B.M. Butcher, J.R. Holland, and C.H. Karnes, p. 33, plenum Press (1973).

16. H.B. Huntington, The Elastic Constants of Crystals, p. 63, Academic Press (1958).

17. J.F. Nye, Physical Properties of Crystals, p. 145, Oxford University Press (1960).

TABLE 1

Transit Times and Probabilities

Outcome	Total Time ($\times 10^{-9}$ sec)	Configurations $\left(\frac{n!}{n_1!n_2!n_3!}\right)$	Probability		Configurations X Probability
$10t_1$	19.970	1	p_1^{10}	0.0004334	0.0004334
$9t_1 + t_2$	19.539	10	$p_1^9 p_2$	0.0002172	0.0021720
$8t_1 + 2t_2$	19.108	45	$p_1^8 p_2^2$	0.0001088	0.0048960
$7t_1 + 3t_2$	18.677	120	$p_1^7 p_2^3$	0.0000545	0.0065400
$6t_1 + 4t_2$	18.246	210	$p_1^6 p_2^4$	0.0000273	0.0057330
$5t_1 + 5t_2$	17.815	252	$p_1^5 p_2^5$	0.0000136	0.0034272
$4t_1 + 6t_2$	17.384	210	$p_1^4 p_2^6$	0.0000068	0.0014280
$3t_1 + 7t_2$	16.953	120	$p_1^3 p_2^7$	0.0000034	0.0004080
$2t_1 + 8t_2$	16.522	45	$p_1^2 p_2^8$	0.0000017	0.0000765
$1t_1 + 9t_2$	16.091	10	$p_1 p_2^9$	0.0000008	0.0000080
$10t_2$	15.660	1	p_2^{10}	0.0000004	0.0000004
$9t_2 + t_3$	16.407	10	$p_2^9 p_3$	0.0000005	0.0000050
$8t_2 + 2t_3$	17.154	45	$p_2^8 p_3^2$	0.0000007	0.0000315
$7t_2 + 3t_3$	17.901	120	$p_2^7 p_3^3$	0.0000010	0.0001200
$6t_2 + 4t_3$	18.648	210	$p_2^6 p_3^4$	0.0000013	0.0002730

TABLE 1 (contd)

$5t_2 + 5t_3$	19.395	252	$p_2^5 p_3^5$	0.0000018	0.0004536
$4t_2 + 6t_3$	20.142	210	$p_2^4 p_3^6$	0.0000024	0.0005040
$3t_2 + 7t_3$	20.889	120	$p_2^3 p_3^7$	0.0000032	0.0003840
$2t_2 + 8t_3$	21.636	45	$p_2^2 p_3^8$	0.0000043	0.0001935
$t_2 + 9t_3$	22.383	10	$p_2 p_3^9$	0.0000057	0.0000570
$10t_3$	23.130	1	p_3^{10}	0.0000076	0.0000076
$9t_3 + t_1$	22.814	10	$p_3^9 p_1$	0.0000114	0.0001140
$8t_3 + 2t_1$	22.498	45	$p_3^8 p_1^2$	0.0000171	0.0007695
$7t_3 + 3t_1$	22.182	120	$p_3^7 p_1^3$	0.0000257	0.0030840
$6t_3 + 4t_1$	21.866	210	$p_3^6 p_1^4$	0.0000385	0.0080850
$5t_3 + 5t_1$	21.550	252	$p_3^5 p_1^5$	0.0000577	0.0145404
$4t_3 + 6t_1$	21.234	210	$p_3^4 p_1^6$	0.0000863	0.0181230
$3t_3 + 7t_1$	20.918	120	$p_3^3 p_1^7$	0.0001292	0.0155040
$2t_3 + 8t_1$	20.602	45	$p_3^2 p_1^8$	0.0001935	0.0087075
$t_3 + 9t_1$	20.286	10	$p_3 p_1^9$	0.0002896	0.0028960
$8t_1 + t_2 + t_3$	19.855	90	$p_1^8 p_2 p_3$	0.0001450	0.0130500
$7t_1 + 2t_2 + t_3$	19.424	360	$p_1^7 p_2^2 p_3$	0.0000727	0.0261720
$6t_1 + 3t_2 + t_3$	18.993	840	$p_1^6 p_2^3 p_3$	0.0000364	0.0305760

TABLE 1 (contd)

$5t_1 + 4t_2 + t_3$	18.562	1260	$p_1^5 p_2^4 p_3$	0.0000182	0.022932
$8t_2 + t_3 + t_1$	16.838	90	$p_2^8 p_3 p_1$	0.0000011	0.000099
$7t_2 + 2t_3 + t_1$	17.585	360	$p_2^7 p_3^2 p_1$	0.0000015	0.000540
$6t_2 + 3t_3 + t_1$	18.332	840	$p_2^6 p_3^3 p_1$	0.0000020	0.001680
$5t_2 + 4t_3 + t_1$	19.079	1260	$p_2^5 p_3^4 p_1$	0.0000027	0.003402
$8t_3 + t_1 + t_2$	22.067	90	$p_3^8 p_1 p_2$	0.0000085	0.000765
$7t_3 + 2t_1 + t_2$	21.751	360	$p_3^7 p_1^2 p_2$	0.0000128	0.004608
$6t_3 + 3t_1 + t_2$	21.435	840	$p_3^6 p_1^3 p_2$	0.0000193	0.016212
$5t_3 + 4t_1 + t_2$	21.119	1260	$p_3^5 p_1^4 p_2$	0.0000288	0.036288
$7t_1 + t_2 + 2t_3$	20.171	360	$p_1^7 p_2 p_3^2$	0.0000969	0.034884
$6t_1 + 2t_2 + 2t_3$	19.740	1260	$p_1^6 p_2^2 p_3^2$	0.0000485	0.061110
$5t_1 + 3t_2 + 2t_3$	19.309	2520	$p_1^5 p_2^3 p_3^2$	0.0000243	0.061236
$4t_1 + 4t_2 + 2t_3$	18.878	3150	$p_1^4 p_2^4 p_3^2$	0.0000121	0.038115
$7t_2 + t_3 + 2t_1$	17.269	360	$p_2^7 p_3 p_1^2$	0.0000022	0.000792
$6t_2 + 2t_3 + 2t_1$	18.016	1260	$p_2^6 p_3^2 p_1^2$	0.0000030	0.003780
$5t_2 + 3t_3 + 2t_1$	18.763	2520	$p_2^5 p_3^3 p_1^2$	0.0001397	0.010080
$4t_2 + 4t_3 + 2t_1$	19.510	3150	$p_2^4 p_3^4 p_1^2$	0.0000054	0.017010
$7t_3 + t_1 + 2t_2$	21.320	360	$p_3^7 p_1 p_2^2$	0.0000640	0.002304

TABLE 1 (contd)

$6t_3 + 2t_1 + 2t_2$	21.004	1260	$p_3^6 p_1^2 p_2^2$	0.0000096	0.012096
$5t_3 + 3t_1 + 2t_2$	20.688	2520	$p_3^5 p_1^3 p_2^2$	0.0000144	0.036288
$4t_3 + 4t_1 + 2t_2$	20.372	3150	$p_3^4 p_1^4 p_2^2$	0.0000216	0.068040
$6t_1 + t_2 + 3t_3$	20.487	840	$p_1^6 p_2 p_3^3$	0.0000647	0.054348
$5t_1 + 2t_2 + 3t_3$	20.056	2520	$p_1^5 p_2^2 p_3^3$	0.0000324	0.081648
$4t_1 + 3t_2 + 3t_3$	19.625	4200	$p_1^4 p_2^3 p_3^3$	0.0000161	0.067620
$6t_2 + t_3 + 3t_1$	17.700	840	$p_2^6 p_3 p_1^3$	0.0000045	0.003780
$5t_2 + 2t_3 + 3t_1$	18.447	2520	$p_2^5 p_3^2 p_1^3$	0.0000061	0.015372
$4t_2 + 3t_3 + 3t_1$	19.194	4200	$p_2^4 p_3^3 p_1^3$	0.0000831	0.034020
$6t_3 + t_1 + 3t_2$	20.573	840	$p_3^6 p_1 p_2^3$	0.0000048	0.004032
$5t_3 + 2t_1 + 3t_2$	20.257	2520	$p_3^5 p_1^2 p_2^3$	0.0000072	0.018144
$4t_3 + 3t_1 + 3t_2$	19.941	4200	$p_3^4 p_1^3 p_2^3$	0.0000108	0.045360
$6t_1 + t_2 + 3t_3$	20.487	840	$p_1^6 p_2 p_3^3$	0.0000647	0.054348
$5t_1 + t_2 + 4t_3$	20.803	1260	$p_1^5 p_2 p_3^4$	0.0000432	0.054432
$4t_1 + 2t_2 + 4t_3$	20.372	3150	$p_1^4 p_2^2 p_3^4$	0.0000216	0.068040
$5t_2 + t_3 + 4t_1$	18.131	1260	$p_2^5 p_3 p_1^4$	0.0000091	0.011466
$4t_2 + 2t_3 + 4t_1$	18.878	3150	$p_2^4 p_3^2 p_1^4$	0.0000121	0.038115

TOTAL: 1.0533601

TABLE 2

Pressures at the Front for the Different Crystallografic Orientations in the First Three Grain Layers.

First Grain Layer		Second Grain Layer		Third Grain Layer	
Orientation	Pressure	Orientation	Pressure	Orientation	Pressure
				100	275
		100	275	110	310
				111	335
				100	272
100	275	110	310	110	310
				111	337
				100	268
		111	335	110	303
				111	335
				100	270
		100	270	110	305
				111	330
				100	270
110	308	110	308	110	308
				111	335
				100	268
		111	335	110	303
				111	335
				100	265
		100	265	110	300
				111	325
				100	262
111	332	110	300	110	300
				111	328
				100	265
		111	332	110	300
				111	332

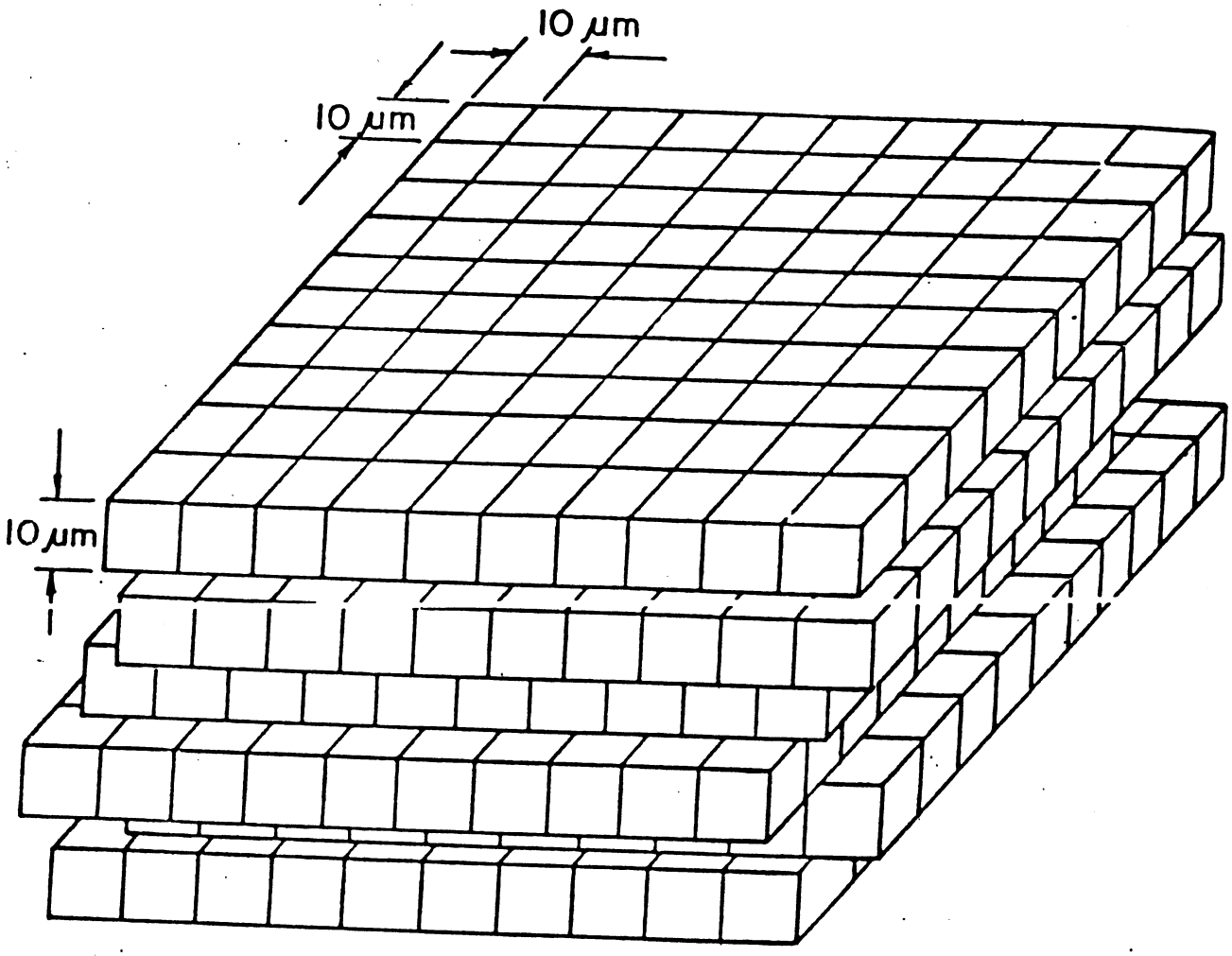

Figure 1. Simplified Configuration for the Grains.

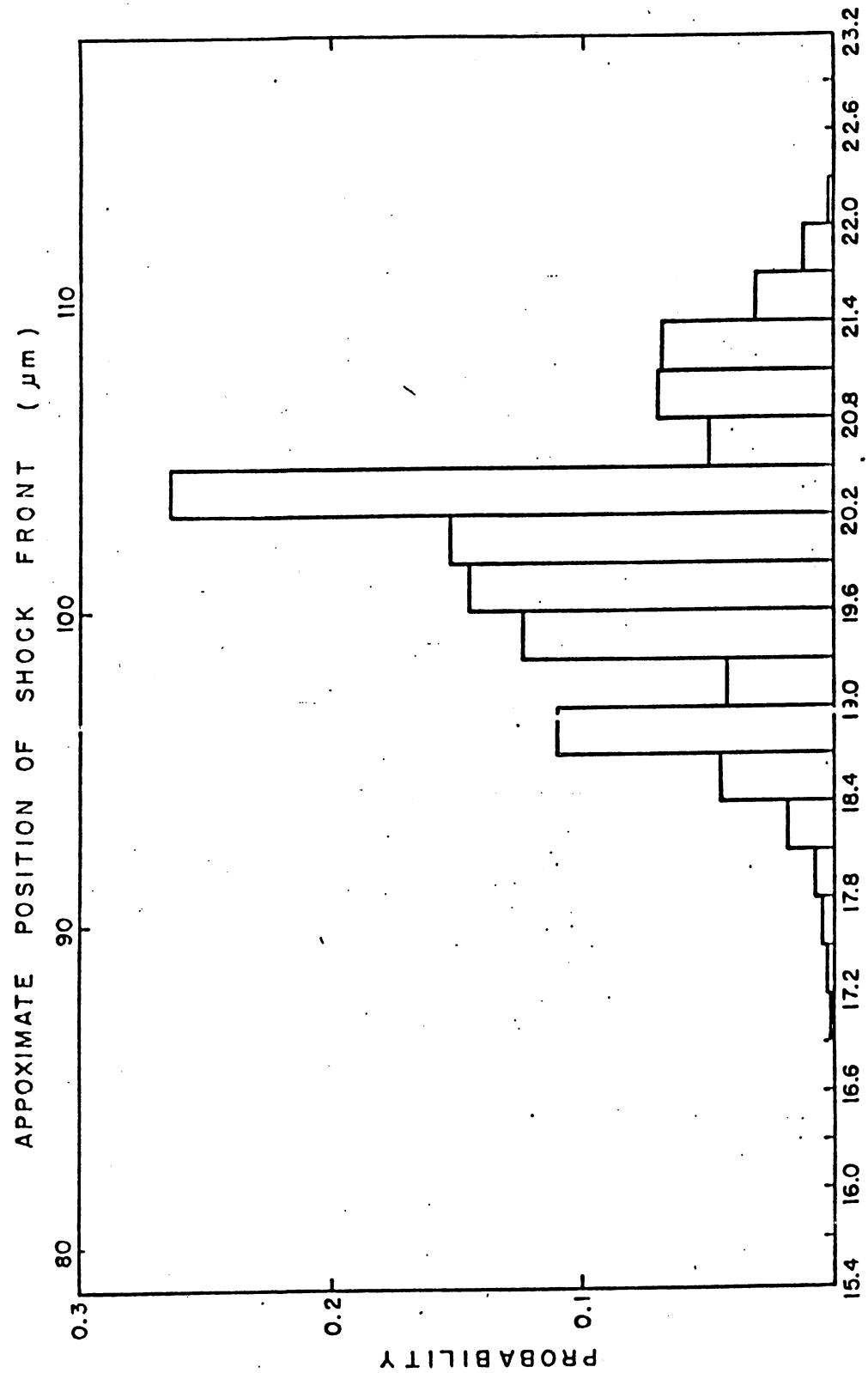

Figure 2. Distributions of Transit Times and Shock Front Positions.

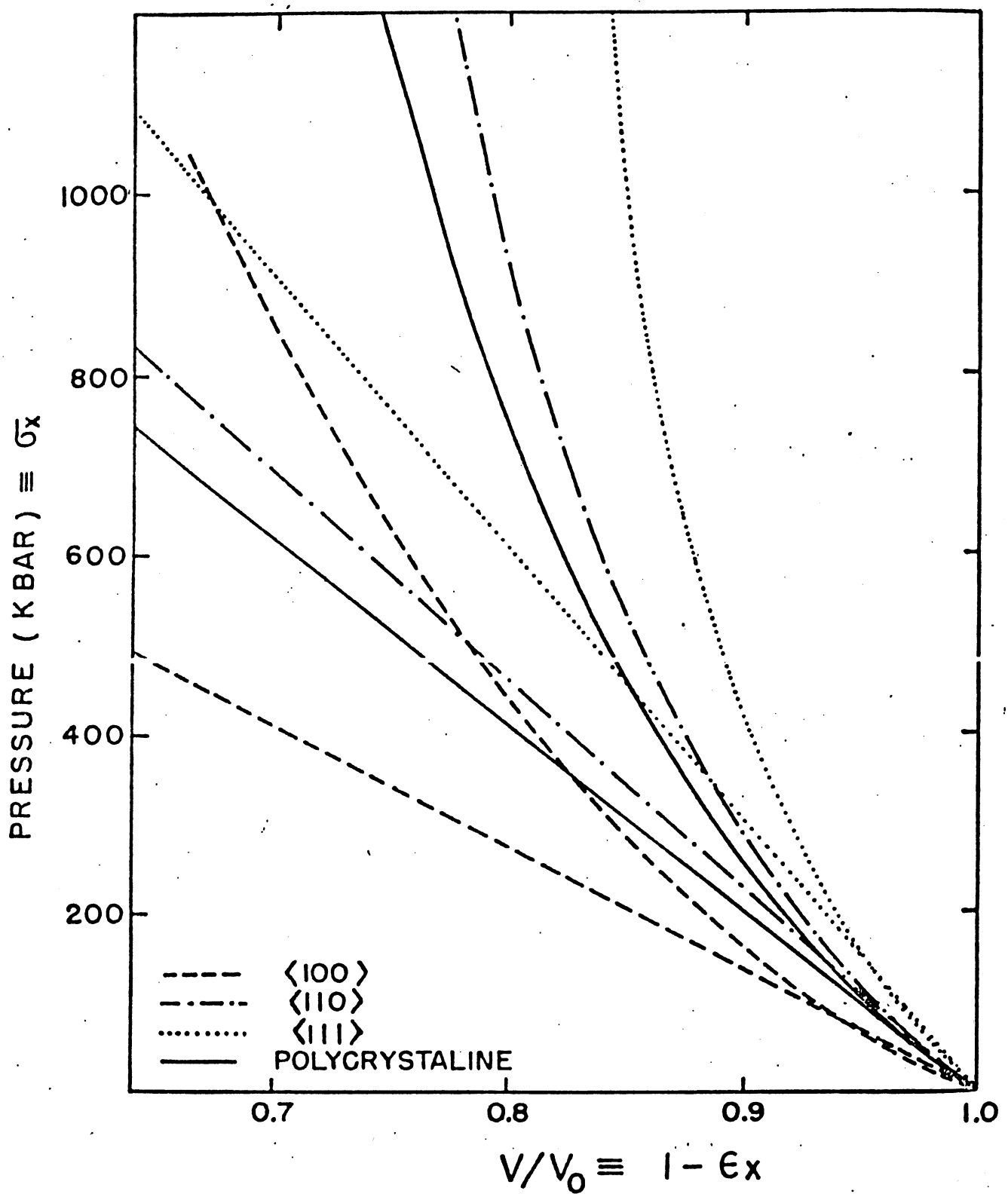

Figure 3. Hugoniot Curves for the Three Crystallografic Orientations and Polycrystalline Nickel.

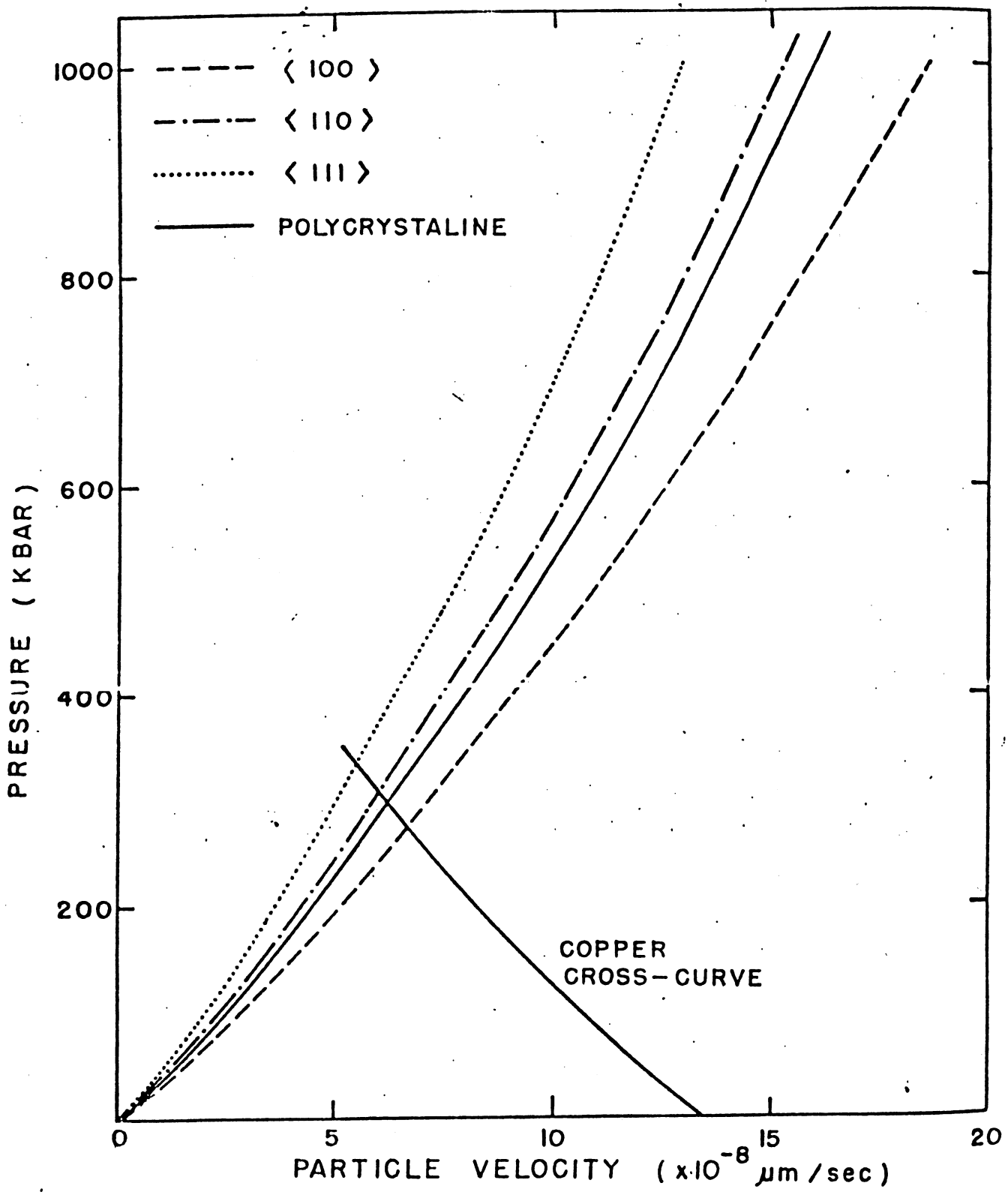

Figure 4. Pressure-Particle Velocity Curves for the Three Crystallografic Orientations and Polycrystalline Nickel and Copper Cross-Curve for 300 Kbar.

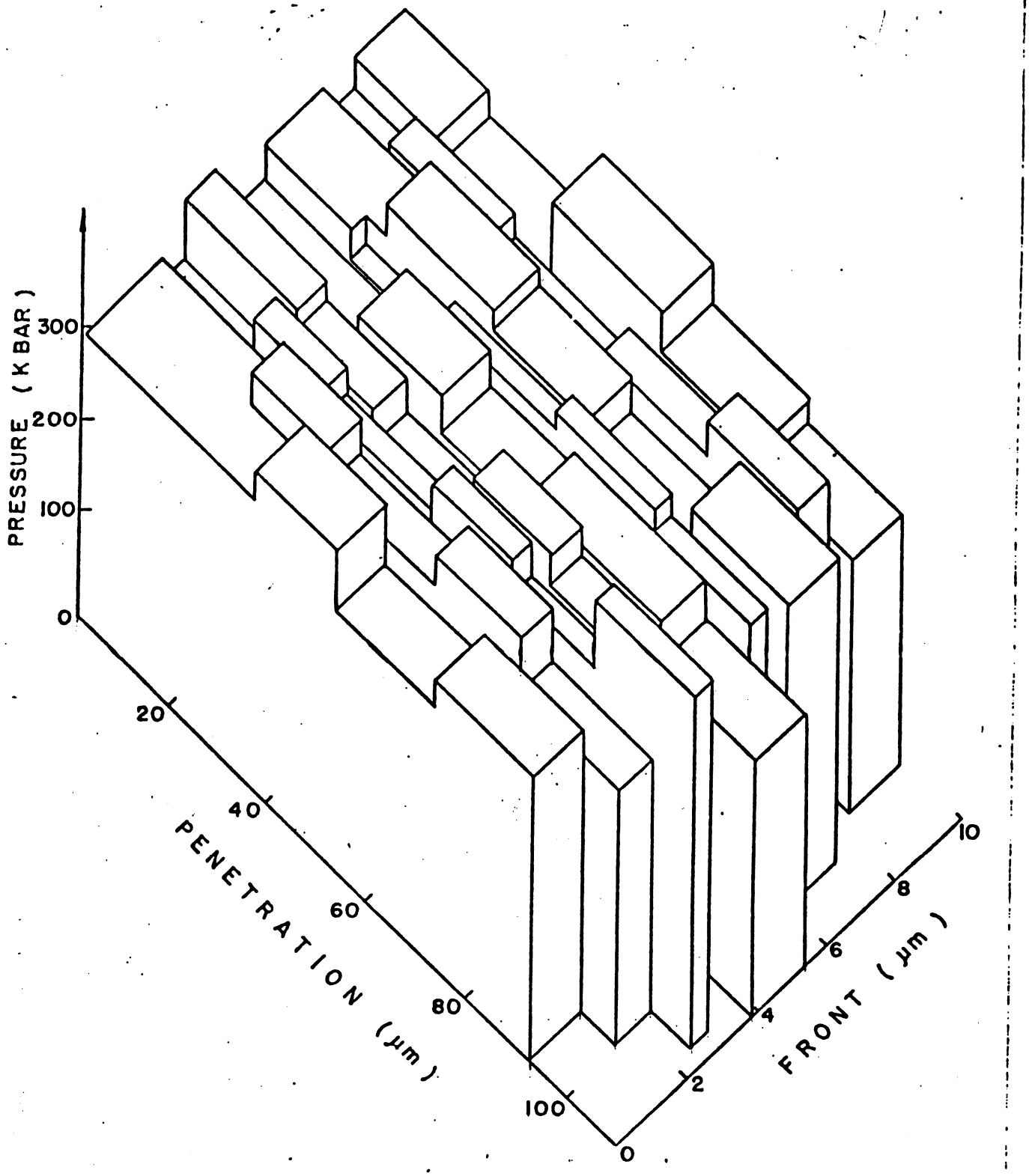

Figure 5. Proposed Model for Shock Wave (Shock Front at about 100 μm below Surface).